

A NUMERICAL METHOD FOR ELECTROMAGNETIC SCATTERING FROM DIELECTRIC ROUGH SURFACES BASED ON THE STOCHASTIC SECOND DEGREE METHOD

Y. Du and B. Liu

The Department of Information Science and Electronics Engineering
Zhejiang University
Hangzhou 310027, China

Abstract—In this paper, we propose an iterative numerical approach based on the stochastic second degree (SSD) algorithm in combination with a new splitting of the impedance matrix to analyze electromagnetic scattering from 1-D dielectric rough surfaces. The embedded matrix-vector product is computed using the banded matrix iterative approach/canonical grid (BMIA/CAG) and the spectral acceleration (SA) technique. For Gaussian surface with Gaussian spectrum, through extensive numerical simulation, it is observed that for HH polarization, the proposed method requires roughly one half number of iterations as needed by the forward-backward method with spectral acceleration (FBM-SA). When the *rms* height is small, the proposed method takes more run time; when the *rms* slope is no less than 0.33 and *rms* height is no less than 1.0λ , where λ is the wavelength, the proposed method is more efficient. More importantly, it obviously improves the convergence properties over FBM-SA by changing cases from divergent to convergent when *rms* height is no less than 2.0λ and *rms* slope is no less than 0.55 except for one extreme case. For VV polarization, the proposed method is less computationally efficient in terms of run time and number of iterations than FBM-SA. However, as far as convergence properties are considered, similar to HH polarization, the proposed method improves over FBM-SA when the *rms* height and *rms* slope are large. Hence for both polarizations, the proposed method demonstrates its suitability when dealing with truly rough surfaces.

Corresponding author: Y. Du (zjydu03@zju.edu.cn).

1. INTRODUCTION

Electromagnetic scattering from randomly rough surfaces is an important research topic in remote sensing (e.g., [1–6]). Several fast numerical techniques have been proposed in the literature for both one-dimensional and two-dimensional rough surfaces. For two dimensional surfaces, one popular method is the sparse matrix/canonical grid (SMCG) iterative method [7]. This approach is computationally efficient for matrix-vector product, either involving sparse matrix or through the fast Fourier transform (FFT). For PEC surfaces, another efficient method was recently proposed by the authors which was based on the stochastic second degree (SSD) method [8] to solve the optimal structural parameter s which minimizes the expected spectral radius, in combination with the efficient approach for computing the matrix-vector product as embedded in the SMCG method. Since for PEC surfaces, the impedance matrix generated from the magnetic field integral equation (MFIE) is diagonally dominated by values around $1/2$, a new matrix-splitting scheme was also used to facilitate the solution of the inner iteration and in the meanwhile to maintain a reasonably good convergence rate. Desirable stability is observed in terms of run time increase due to increase of the number of surface unknowns. The above methods are efficient for analyzing scattering from surfaces with small to moderate roughness.

For large roughness, we proposed a new algorithm [9], which combines the SSD iterative method with the sparse matrix (SM) algorithm to achieve high computational efficiency, and further uses the Chebyshev approximation to replace the Taylor expansion for the weak interaction between two points beyond mutual neighborhoods. Numerical example demonstrates the suitability of the proposed method for rough surfaces with *rms* height larger than 3 wavelengths.

However, when the rough surfaces under consideration are dielectric, things become more complicated. Two Greens functions are required for the two media problem. And a much denser discretization of the surface for the dielectric medium may be required because the wavenumber can be much larger than that of the free-space. In turn the CPU and memory requirement is much more demanding. To reduce CPU time, in [10] a physics-based two-grid method (PBTG) was proposed, where two kinds of grids are used, namely, a dense grid and a sparse grid. The sparse grid is the usual sampling grid of free space, while the dense grid depends on the wavenumber of the dielectric medium.

Since fields in the two media need to be analyzed simultaneously, the impedance matrix generated from the field integral equation

becomes more complex by containing information of both media. Moreover, it loses the special form attained by its PEC counterpart where the diagonal elements are dominated by values around $1/2$.

Nevertheless, an appropriate splitting of the impedance matrix is of critical importance in constructing an iterative solution to the linear system. Not only the choice of splitting determines the asymptotic convergence rate of the iterative system, but it determines if the iterative system converges or diverges. There are different splitting schemes proposed within the SMCG technique [11]. For 1D rough surfaces, the most popular methods, such as the banded matrix iterative approach/canonical grid (BMIA/CAG) [12] for PEC rough surface, the physics-based two-grid method (PBTG) [10, 13] for dielectric rough surface, and the iterative forward-backward method (FBM) for both PEC [14] and dielectric rough surfaces [15], represent different choice of the splitting [16].

In analyzing EM scattering from 1-D dielectric rough surfaces, recently we proposed an efficient and accurate iterative numerical approach [17]. It is based on a new splitting of the impedance matrix Z to improve the asymptotic convergence rate of the resultant iterative system. The structure of split matrix is then fully explored, in combination with the application of an identity for inverse of block matrix, to further reduce the computational and storage complexity. The embedded matrix-vector product is computed using the spectral acceleration technique. For Gaussian surface with Gaussian spectrum, it converges faster than both forward-backward method (FBM) and FBM with spectral acceleration (FBM-SA) [18].

Before attacking the more complicated three-dimensional scattering from 2D dielectric rough surfaces, in the current work we choose to build on our previous study on scattering from 1D dielectric rough surfaces, where the SSD iterative algorithm is applied.

The remainder of this paper is organized as follows. In Section 2, we describe our numerical approach, which is based on the SSD in combination with a new matrix splitting method and of SA. Numerical analysis of the computational efficiency and convergence properties of the proposed method is presented in Section 3. Section 4 concludes this paper.

2. FORMULATION

Consider a tapered plane wave $\psi_{\text{inc}}(x, z)$ incident upon a one-dimensional (1D) dielectric rough surface. The random height profile is $z = f(x)$. The upper medium has relative dielectric constant ε and permeability μ . The lower medium has relative dielectric constant ε_1

and permeability μ_1 . The fields ψ in the upper medium and ψ_1 in the lower medium satisfy the following surface integral equations [11]

$$\frac{1}{2}\psi(\bar{r}') - \int_s \left[\psi(\bar{r}) \frac{\partial G(\bar{r}, \bar{r}')}{\partial n} - G(\bar{r}, \bar{r}') \frac{\partial \psi(\bar{r})}{\partial n} \right] ds = \psi_{inc}(\bar{r}') \quad (1)$$

$$\frac{1}{2}\psi_1(\bar{r}') + \int_s \left[\psi_1(\bar{r}) \frac{\partial G_1(\bar{r}, \bar{r}')}{\partial n} - G_1(\bar{r}, \bar{r}') \frac{\partial \psi_1(\bar{r})}{\partial n} \right] ds = 0 \quad (2)$$

where the point $\bar{r} = \hat{x}x + \hat{z}f(x)$ is on the surface with unit surface norm \hat{n} pointing upward; G is the 2D Green's function in the upper medium and G_1 in the lower medium; f denotes the Cauchy principle value integral.

The boundary conditions are $\psi(\bar{r}) = \psi_1(\bar{r})$ and $\partial\psi(\bar{r})/\partial n = \mu_1/\mu\partial\psi_1(\bar{r})/\partial n$ for TE case, and are $\psi(\bar{r}) = \psi_1(\bar{r})$ and $\partial\psi_1(\bar{r})/\partial n = \varepsilon_1/\varepsilon\partial\psi(\bar{r})/\partial n$ for TM case. The second condition can be put in a more compact form as $\partial\psi_1(\bar{r})/\partial n = \rho\partial\psi(\bar{r})/\partial n$ where $\rho = \mu_1/\mu$ or $\varepsilon_1/\varepsilon$ for TE or TM case, respectively.

After discretization, (1) and (2) become

$$\sum_{n=1}^N a_{mn}u(x_n) + \sum_{n=1}^N b_{mn}\psi(x_n) = \psi_{inc}(x_m) \quad (3)$$

$$\sum_{n=1}^N c_{mn}\rho u(x_n) + \sum_{n=1}^N d_{mn}\psi(x_n) = 0 \quad (4)$$

where $u(x) = \sqrt{1 + [f'(x)]^2}\partial\psi/\partial n$. The matrix elements a_{mn} , b_{mn} , c_{mn} and d_{mn} are [11]

$$a_{mn} = \begin{cases} \Delta x \frac{i}{4} H_0^{(1)}(kr_{mn}) & m \neq n \\ \Delta x \frac{i}{4} H_0^{(1)}[k\Delta x\gamma_m/(2e)] & m = n \end{cases} \quad (5)$$

$$b_{mn} = \begin{cases} -\Delta x \frac{ik}{4} \frac{f'(x_n)(x_n-x_m) - [f(x_n) - f(x_m)]}{r_{mn}} & m \neq n \\ H_1^{(1)}(kr_{mn}) & m = n \\ \frac{1}{2} - \frac{f''(x_m)\Delta x}{4\pi\gamma_m^2} & m \neq n \end{cases} \quad (6)$$

$$c_{mn} = \begin{cases} -\Delta x \frac{i}{4} H_0^{(1)}(k_1r_{mn}) & m \neq n \\ -\Delta x \frac{i}{4} H_0^{(1)}[k_1\Delta x\gamma_m/(2e)] & m = n \end{cases} \quad (7)$$

$$d_{mn} = \begin{cases} \Delta x \frac{ik_1}{4} \frac{f'(x_n)(x_n-x_m) - [f(x_n) - f(x_m)]}{r_{mn}} & m \neq n \\ H_1^{(1)}(k_1r_{mn}) & m = n \\ \frac{1}{2} + \frac{f''(x_m)\Delta x}{4\pi\gamma_m^2} & m \neq n \end{cases} \quad (8)$$

where $r_{mn} = \sqrt{(x_n - x_m)^2 + [f(x_n) - f(x_m)]^2}$, $\gamma_m = \sqrt{1 + [f'(x_m)]^2}$, Δx is the x -distance of two consecutive points on the surface. $H_n^{(1)}(\cdot)$

denotes the Hankel function of the first kind. k and k_1 are the free-space propagation constants of the upper and lower media, respectively.

The discretized system can be expressed more compactly in matrix and vector form as

$$\overline{\overline{Z}}\overline{\overline{x}} = \overline{\overline{b}} \tag{9}$$

where $\overline{\overline{Z}} = \begin{pmatrix} \overline{\overline{Z}}_a & \overline{\overline{Z}}_b \\ \overline{\overline{Z}}_c & \overline{\overline{Z}}_d \end{pmatrix}$, $\overline{\overline{x}} = \begin{pmatrix} \overline{U} \\ \overline{\psi} \end{pmatrix}$, and $\overline{\overline{b}} = \begin{pmatrix} \overline{\psi}_{inc} \\ 0 \end{pmatrix}$.

2.1. The Proposed Method

2.1.1. A New Splitting of the Impedance Matrix

In [17], $\overline{\overline{Z}}$ is split into a easy-to-invert matrix $\overline{\overline{M}}$ and the remainder $\overline{\overline{N}}$, that is, $\overline{\overline{Z}} = \overline{\overline{M}} - \overline{\overline{N}}$. A corresponding iterative sequence is formed as

$$\overline{\overline{M}}\overline{\overline{x}}_{k+1} = \overline{\overline{N}}\overline{\overline{x}}_k + \overline{\overline{b}} \tag{10}$$

where $k = 0, 1, 2, \dots$, or equivalently put it as

$$\overline{\overline{x}}_{k+1} = \overline{\overline{B}}\overline{\overline{x}}_k + \tilde{\overline{\overline{b}}} \tag{11}$$

where $\overline{\overline{B}} = \overline{\overline{M}}^{-1}\overline{\overline{N}}$ and $\tilde{\overline{\overline{b}}} = \overline{\overline{M}}^{-1}\overline{\overline{b}}$. The form of $\overline{\overline{M}}$ that we use in this study is

$$\overline{\overline{M}} = \begin{pmatrix} 1/2 & 0 & \cdots & 0 \\ \overline{\overline{Z}}_a^s + \overline{\overline{Z}}_a^{FS} & 0 & 1/2 & \ddots & \vdots \\ \vdots & \ddots & \ddots & \ddots & 0 \\ 0 & \cdots & 0 & 1/2 & \vdots \\ 1/2 & 0 & \cdots & 0 & 0 \\ \overline{\overline{Z}}_c^s & 0 & 1/2 & \ddots & \vdots \\ \vdots & \ddots & \ddots & \ddots & 0 \\ 0 & \cdots & 0 & 1/2 & 0 \end{pmatrix} \tag{12}$$

Determination of this form for $\overline{\overline{M}}$ is based on the observation that the impedance matrix $\overline{\overline{Z}}$ is characteristically composed of four subblocks (see (9)), with each representing different types of interactions among points on the surface. The subblocks $\overline{\overline{Z}}_b$ and $\overline{\overline{Z}}_d$ are special in that they are diagonally dominated by the value of one half. This observation motivates us to follow the way of matrix splitting in [8, 9]. The way of splitting the subblock $\overline{\overline{Z}}_a$ is similar to the BMIA/CAG approach, where a three-part partition is carried out, and the strong

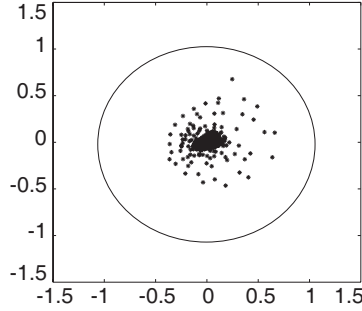


Figure 1. Spectrum of the iteration matrix $\overline{\overline{B}}$.

part $\overline{\overline{Z}}_a^s$ and canonical grid weak part $\overline{\overline{Z}}_a^{FS}$ are kept in $\overline{\overline{M}}$. Similar treatment is applied to the subblock $\overline{\overline{Z}}_c$. Yet for this subblock some simplification can be performed, specifically, the weak part is ignored, since it is related to the Green’s function in the lower region which can demonstrate moderate to large attenuation [11]. This form of matrix splitting has the desirable property of keeping the computational complexity manageable.

For such sequence to converge for an arbitrary initial $\overline{\overline{x}}_0$, it must hold that $\rho(\overline{\overline{B}}) < 1$, where $\rho(\overline{\overline{B}})$ is the spectral radius of $\overline{\overline{B}}$. We now examine the convergence property of the proposed iterative system. Fig. 1 provides one illustration of the spectrum of iteration matrix $\overline{\overline{B}}$ for HH polarization, where a 1D dielectric rough surface is considered, which follows a Gaussian process with Gaussian spectrum. The *rms* height is $\sigma = 1.5\lambda$, and the correlation length is $lc = 3\lambda$, with λ being the wavelength. The relative dielectric constant is $\epsilon_r = 15 + 4i$. The total number of unknowns is 3000. The spectral radius is 0.72, corresponding to an asymptotic convergence rate of 0.14. This rate is appealing considering the fact that in this case the surface is very rough. Further numerical experiments also show satisfactory results.

2.1.2. SSD Formulation

Corresponding to the first order iterative system (10), the SSD iterative sequence is

$$\overline{\overline{M}}\overline{\overline{x}}_{k+2} = -\mu\overline{\overline{Z}} \left(\frac{1}{s+1}\overline{\overline{x}}_{k+1} + \frac{s}{s+1}\overline{\overline{x}}_k \right) + \overline{\overline{M}}((1-s)\overline{\overline{x}}_{k+1} + s\overline{\overline{x}}_k) + \mu\overline{\overline{b}} \quad (13)$$

where s is a structural parameter to be optimized; μ is a controlling parameter for the Jacobi-Richardson shift $\overline{\overline{B}} = \mu\overline{\overline{B}} + (1-\mu)\overline{\overline{I}}$; $\overline{\overline{B}}$ is

the iteration matrix of the first-degree system; \bar{I} is the $N \times N$ identity matrix. Here μ takes the value of one half. The optimal s_0 is found to be the solution to the following equation [8]

$$\int^s s \frac{\partial f_N(w)}{\partial s} dw + \int_s \left(f_N(w) + w \frac{\partial f_N(w)}{\partial s} \right) dw = 0. \quad (14)$$

where $f_N(w)$ is the probability density of the largest order statistic $w_N \triangleq \max_{\lambda_k \in \sigma(\bar{B})} (g_k(s) := \frac{|\lambda_k - s|}{1 - s})$, and $\sigma(\bar{B})$ is the spectrum of \bar{B} .

In (13), the product of the impedance matrix \bar{Z} with a vector can be computed using a highly efficient algorithm as embedded in SA. The inner iteration of (13) can be symbolically put as

$$\bar{M}\bar{x}_{k+2} = \bar{v} + \bar{M}\bar{u}. \quad (15)$$

The system $\bar{M}\bar{x}_{k+2} = \bar{v}$ is solved per our fast algorithm [17], which makes use of our matrix-splitting scheme

$$\bar{M} = \begin{pmatrix} \bar{M}_{11} & \bar{M}_{12} \\ \bar{M}_{21} & \bar{M}_{22} \end{pmatrix}, \quad \bar{v} = \begin{pmatrix} \bar{v}_1 \\ \bar{v}_2 \end{pmatrix}, \quad (16)$$

where the property that both \bar{M}_{12} and \bar{M}_{21} are both diagonal matrices are to be fully exploited,

$$\bar{M}_{12} = 1/2\bar{I}, \quad \bar{M}_{21} = 1/2\bar{I}. \quad (17)$$

The fast algorithm is formulated as follows:

- 1) Let $\bar{d} = \bar{v}_2 - \bar{v}_1$.
- 2) Calculate $\bar{D} = \bar{M}_{11} - \bar{M}_{21}$.
- 3) Solve $\bar{D}\bar{w} = \bar{d}$
- 4) Form $\left[\begin{matrix} -\bar{w} \\ 2\bar{v}_2 + 2\bar{M}_{21}\bar{w} \end{matrix} \right]$, which is the solution \bar{x}_{k+2} .

In this algorithm, the original system $\bar{M}\bar{x}_{k+2} = \bar{v}$ is replaced by the new system $\bar{D}\bar{w} = \bar{d}$, resulting in a dimension reduction from N to $N/2$.

Now it follows that the inner solution to (15) is

$$\bar{x}_{k+2} = \bar{x}_{k+2} + \bar{u} \quad (18)$$

2.1.3. Spectral Acceleration

In evaluating the product of the impedance matrix $\overline{\overline{Z}}$ with a vector, the spectral acceleration algorithm is one of several efficient approaches and is adopted in this study. The basic concepts of the SA algorithm are given as follows. Interested readers may refer to [19] for more details.

Let $E^{f,(i)}, E^{b,(i)}, i = (1, 2)$ denote the forward and backward radiation by the source current elements, where the superscript i refers to the medium above the surface ($i = 1$) or below ($i = 2$). $E^{f,(1)}(x_n)$ has two components, namely, the strong and weak parts, as follows

$$E^{f,(1)}(x_n) = E^{fs,(1)}(x_n) + E^{fw,(1)}(x_n) = \sum_{m=n-N_s}^{n-1} \left(Z_{mn}^{(a)} U_m + Z_{mn}^{(b)} \psi_m \right) + \sum_{m=1}^{n-N_s-1} \left(Z_{mn}^{(a)} U_m + Z_{mn}^{(b)} \psi_m \right) \quad (19)$$

The strong term $E^{fs,(1)}(x_n)$ is calculated by direct matrix-vector product using exact matrix elements. The weak contribution $E^{fw,(1)}(x_n)$ is obtained by employing the spectral representation of the Green's function [19], and it is expressed as

$$E^{fw,(1)}(x_n) = \sum_{m=1}^{n-N_s-1} \left(Z_{mn}^{(a)} U_m + Z_{mn}^{(b)} \psi_m \right) = \frac{i\Delta x}{4\pi} \int_{C_\theta} F_n(\theta) e^{ikz_n \sin \theta} d\theta, \quad (20)$$

where $F_n(\theta)$ can be calculated from weak element currents through a recursive procedure

$$F_n(\theta) = F_{n-1}(\theta) e^{ik\Delta x \cos \theta} + [-ik(-\sin \theta + f_{x_m} \cos \theta) U_{n-N_s-1} + \psi_{n-N_s-1}] \times e^{ik(N_s+1)\Delta x \cos \theta} e^{-ikz_{n-N_s-1} \sin \theta} \quad (21)$$

The other quantities, $E^{f,(2)}$ and $E^{b,(i)}$, $i = (1, 2)$, can be treated similarly.

2.2. Complexity Analysis

For outer iteration of (13), to update the right side a matrix-vector product $\overline{\overline{Z}}\overline{y}_{k+1}$ needs to be computed, where $\overline{y}_{k+1} = \frac{1}{s+1}\overline{x}_{k+1} + \frac{s}{s+1}\overline{x}_k$. This product can be efficiently computed using SA. Therefore,

updating the right side (exclusive of the term $\overline{\overline{M}}((1-s)\overline{x}_{k+1} + s\overline{x}_k)$ for it is separately added as shown in (15)) in the outer iteration requires $O(N) + O(bw \times N)$ operations, where the latter term is related to the strong part needed in SA. The inner iteration is solved by means of the Krylov-subspace based algorithm GMRES for reasons as stated in [8]. Since in the proposed approach the dimensionality of the inner iteration is reduced by one half as indicated in the formation of the matrix $\overline{\overline{D}}$ in step 3) of the above algorithm, while bandedness plus Toeplitz structure is preserved in $\overline{\overline{D}}$, appreciable computational gain has been achieved compared to BMIA/CAG.

As far as memory efficiency is concerned, comparing to BMIA/CAG, our approach can reduce the storage requirement by more than one half. This is because while BMIA/CAG needs to maintain bandedness for all the four subblocks $\overline{\overline{M}}_{11} \sim \overline{\overline{M}}_{22}$, where the storage for $\overline{\overline{M}}_{11}$ and $\overline{\overline{M}}_{12}$ can be appreciable when the number of unknowns N is large (the neighborhood distance is usually chosen as $N/10$), in our approach the subblocks $\overline{\overline{M}}_{12}$ and $\overline{\overline{M}}_{22}$ are each replaced by a diagonal matrix, hence effectively reduces the storage by one half. Moreover, reduction of the dimensionality of the inner iteration by one half along with the preservation of the banded plus Toeplitz structure of the matrix entails that the storage as required in constructing the Krylov subspace in GMRES is further reduced.

3. NUMERICAL ILLUSTRATIONS

In this section, we evaluate the accuracy and convergence behavior of the proposed method. We also make a comparison with FBM-SA. For notational convenience, in the following we shall call the method proposed in this paper as SSD-NS-SA, standing for the combination of SSD, new matrix splitting, and spectral acceleration. All results are run on a Core 2 with double CPU of 3.0 GHz and memory of 4.0 GB.

In the numerical illustrations, the outer iteration is carried out until the error norm criterion

$$\frac{\|\overline{\overline{Z}}\overline{x}_k - \overline{b}\|}{\|\overline{b}\|} < 10^{-4} \tag{22}$$

is satisfied. The normalized bistatic scattering coefficient (NBSC) is defined as [11]

$$\sigma(\theta_s) = \frac{|\psi_S^{(N)}(\theta_s)|^2}{8\pi k g \sqrt{\frac{\pi}{2}} \cos \theta_i \left[1 - \frac{1+2 \tan^2 \theta_i}{2k^2 g^2 \cos^2 \theta_i} \right]} \tag{23}$$

where g is the tapering parameter; θ_i is the incidence angle; θ_s is the scattering angle, and

$$\psi_S^{(N)}(\theta_s) = - \int_{-\infty}^{\infty} dx \left\{ -U(x) + \psi(x)ik \left[\frac{df}{dx} \sin \theta_s - \cos \theta_s \right] \right\} \cdot e^{-ik(\sin \theta_s x + f(x) \cos \theta_s)} \quad (24)$$

We shall consider Gaussian surface profiles with Gaussian spectrum. The spectrum is

$$W(k) = \frac{h^2 lc}{\sqrt{4\pi}} \exp\left(-\frac{k^2 lc^2}{4}\right) \quad (25)$$

where h is the *rms* height, and lc is the correlation length.

The Green's function in the lower region can have moderate to large attenuation [11]. A medium with a large real part of dielectric constant is normally associated with a large imaginary part. Let r_{mn} be the distance between the m th and the n th parts. When r_{mn} is greater than a certain value, say rl , the field interaction between the m th and the n th point is vanishingly small. In the numerical simulations, rl is fixed at 5λ . The Green's function for the lower medium is set to zero when the distance r_{mn} is larger than rl . This simplification is unnecessary yet can help save some computation. When it is used, $\overline{\overline{Z}}_c$ and $\overline{\overline{Z}}_d$ each becomes a banded matrix.

We start by confirming the accuracy of the proposed method, where we compare the NBSCs obtained by direct matrix inversion (DMI) with that obtained by our method. The surface is a Gaussian surface with Gaussian correlation function, with *rms* height $\sigma = 1.0\lambda$, correlation length $lc = 2.0\lambda$, and relative dielectric constant $\varepsilon_r = 15 + 4i$. The incidence angle is 60° . The tapering parameter is $g = L/4$, where L is the surface length and is set to $L = 64\lambda$. The surface is sampled at 32 points per wavelength, so the total surface unknowns are 4096. The results are averaged over 100 realizations and are shown in Fig. 2. We see that for both HH and VV polarizations, the NBSCs obtained by the proposed method completely overlap with their DMI counterparts.

We then compare run time and number of iterations between SSD-NS-SA and FBM-SA for rough surfaces with different *rms* heights and slopes. The relative dielectric constant, incidence angle are kept the same as before. The number of unknowns is 16384. The *rms* heights ranges from 0.3λ to 3.0λ , and the ratio of *rms* height to correlation length ranges from 0.15 to 1.0, corresponding to *rms* slope from 12° to 55° . All of numerical experiment are averaged over five realizations. If any of the five realizations fails to converge for a specific case, it is

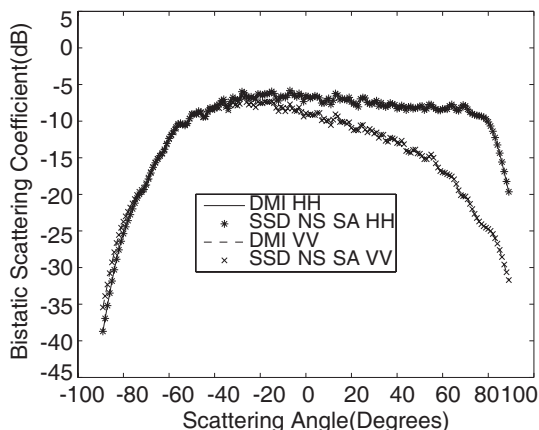


Figure 2. Comparison between the proposed method SSD-NS-SA and DMI of the HH and VV NBSCs from a Gaussian correlated rough surface with $\sigma = 1.0\lambda$ and $lc = 2.0\lambda$

marked with a 'nc' symbol to indicate 'not convergent'. The results for HH polarization are listed in Table 1 for FBM-SA and in Table 2 for SSD-NS-SA using a pair of values, with the one outside the parenthesis denoting run time while the one inside the parenthesis the number of iterations. We observe that SSD-NS-SA reduces the number of iteration by almost one half as required by FBM-SA, which speaks of the effectiveness of the proposed matrix splitting and SSD formalism. However, the efficiency gain in terms of number of iteration is not directly translated to gain in run time. It is seen that when the *rms* slope is 0.33 and *rms* height is no less than 1.0λ that run time of SSD-NS-SA is less than that of FBM-SA. When the *rms* height is small, SSD-NS-SA takes more run time. The disproportion between iteration efficiency and run time efficiency of the proposed method stems from the fact that in the current study, to solve $Dw = d$ in the inner iteration, time-consuming GMRES approach is used.

On the other hand, the improvement of SSD-NS-SA on convergence properties over FBM-SA is impressive when comparing Tables 1 and 2. FBM-SA fails to converge for cases when the *rms* height is no less than 2.0λ and *rms* slope no less than 0.55. The divergence behavior becomes more severe: At higher *rms* slope, FBM-SA tends to diverge at smaller *rms* height. SSD-NS-SA converges for all these cases except for one extreme case. This convergence improvement stems from the Jacobi-Richardson shift, which is currently used in the SSD formalism so as to ensure that

Table 1. FBM-SA. Average run time and number of iterations for different values of *rms* height and slope. Incidence angle: 60° . Relative dielectric constant: $\varepsilon_r = 15 + 4i$. Total number of unknowns is 16384. HH polarization.

σ/lc	$\sigma=0.3$	$\sigma=0.5$	$\sigma=1.0$	$\sigma=2.0$	$\sigma=3.0$
0.15	372(21)	401(21)	456(21)	528(21)	588(21)
0.33	378(21)	412(21)	660(20)	840(20)	960(20)
0.55	403(18)	507(19)	672(19)	nc	nc
0.707	367(20)	405(20)	704(20)	nc	nc
1	516(28)	600(22)	nc	nc	nc

Table 2. SSD-NS-SA. Average run time and number of iterations for different values of *rms* height and slope. Incidence angle: 60° . Relative dielectric constant: $\varepsilon_r = 15 + 4i$. Total number of unknowns is 16384. HH polarization.

σ/lc	$\sigma=0.3$	$\sigma=0.5$	$\sigma=1.0$	$\sigma=2.0$	$\sigma=3.0$
0.15	402(10)	494(10)	473(10)	550(12)	640(13)
0.33	470(10)	517(10)	568(10)	653(12)	743(14)
0.55	547(10)	659(10)	673(10)	846(12)	976(14)
0.707	734(10)	859(10)	850(10)	1043(12)	1235(14)
1	1330(11)	1329(10)	1356(11)	1617(13)	nc

the spectrum of the first degree iterative system is located within the circle centered at $1/2$ with radius $1/2$, a location required by the deterministic second degree system [20]. This shift can bring eigenvalues outside the unit circle on the left plane of the complex spectrum into the unit circle when certain conditions are satisfied by the eigenvalues.

However, there is a cost to pay for adopting the Jacobi-Richardson shift: The reduction of computational efficiency in general, with the realization and severity of the reduction dependent on shape of spectrum of the iteration matrix. This is because, application of the Jacobi-Richardson shift dictates a compression of the spectrum by one half, then a shift to the center $1/2$. When convergence rate of the first degree system (10) is good, i.e., when the spectral radius is much smaller than one, shifting to the center $1/2$ may lead to appreciable increase in spectral radius, an increase that cannot be compensated by applying the SSD optimization procedure, hence slows down the

Table 3. Spectral radius of the iteration matrix $\overline{\overline{B}}$.

N	$\sigma = 0.3\lambda$	$\sigma = 0.5\lambda$	$\sigma = 1.0\lambda$	$\sigma = 2.0\lambda$	$\sigma = 3.0\lambda$
1500	0.427	0.373	0.301	0.207	0.149
3000	0.507	0.459	0.428	0.323	0.288

convergence rate. This analysis becomes more relevant when VV polarization is considered. To make this point clear, we return to study of the spectrum of iteration matrix where Fig. 1 is generated and carry out further numerical experiments with increasing roughness. For HH polarization, the spectral radius of $\overline{\overline{B}}$ increases gracefully with increasing *rms* height. On the contrary, for VV polarization it is surprising to find that the trend is just the opposite. Such behavior is demonstrated in Table 3, where the *rms* slope is 25° . Moreover, we find that the spectral radius for VV polarization is sensitive to the number of unknowns and to the *rms* slope. That is, the rougher the surface, the smaller the spectral radius, hence the more severe impact of the Jacobi-Richardson shift. Of course when *rms* slope and/or *rms* height goes beyond certain threshold, the trend of decreasing spectral radius must reverse, otherwise the spectral radius either goes to zero, which is impossible because then the iteration matrix simply vanishes, or converges to some nonzero value, which is equally impossible because one can hardly find any fundamental theory to back such phenomenon. This point has been numerically verified yet the reason for such behavior is still unclear to us and merits further investigation. Numerical experiments show that for VV polarization, SSD-NS-SA is less computationally efficient in terms of run time and number of iterations than FBM-SA. However, as far as convergence properties are considered, similar to HH polarization, SSD-NS-SA improves over FBM-SA by changing cases from divergent to convergent when the *rms* height and *rms* slope are large.

4. CONCLUSION

In this paper, we have developed an iterative numerical approach based on the SSD algorithm in combination with a new splitting of the impedance matrix to analyze EM scattering from 1-D dielectric rough surfaces. For Gaussian surface with Gaussian spectrum, through extensive numerical simulation, it is observed that for HH polarization, the proposed method SSD-NS-SA requires roughly one half number of iterations as needed by FBM-SA method. When the *rms* height is

small, SSD-NS-SA takes more run time; when the *rms* slope is no less than 0.33 and *rms* height is no less than 1.0λ , where λ is the wavelength, SSD-NS-SA is more efficient. More importantly, SSD-NS-SA obviously improves the convergence properties over FBM-SA by changing cases from divergent to convergent when *rms* height is no less than 2.0λ and *rms* slope is no less than 0.55 except for one extreme case. For VV polarization, SSD-NS-SA is less computationally efficient in terms of run time and number of iterations than FBM-SA. However, as far as convergence properties are considered, similar to HH polarization, SSD-NS-SA improves over FBM-SA when the *rms* height and *rms* slope are large. Hence for both polarizations, the proposed method demonstrates its suitability when dealing with truly rough surfaces.

Identification of alternative procedure for the Jacobi-Richardson shift to improve computational efficiency and meanwhile to maintain good convergency properties is currently under way. Preliminary results are also obtained for Gaussian surface with exponential spectrum. After analyzing the data, new findings will be reported in a future paper.

ACKNOWLEDGMENT

This work was supported by National High Technology “863” Programs of China under Grant No. 2009AA12Z113 and China National Science Foundation under Grant No. 40976107.

REFERENCES

1. Tsang, L., J. A. Kong, and R. T. Shin, *Theory of Microwave Remote Sensing*, Wiley-Interscience, New York, 1985.
2. Liang, D., P. Xu, L. Tsang, Z. Gui, and K.-S. Chen, “Electromagnetic scattering by rough surfaces with large heights and slopes with applications to microwave remote sensing of rough surface over layered media,” *Progress In Electromagnetics Research*, PIER 95, 199–218, 2009.
3. Zhou, L., L. Tsang, V. Jandhyala, and C.-T. Chen, “Studies on accuracy of numerical simulations of emission from rough ocean-like surfaces,” *IEEE Trans. Geoscience and Remote Sensing*, Vol. 39, 1757–1763, 2001.
4. Li, Z.-X., “Bistatic scattering from rough dielectric soil surface with a conducting object with arbitrary closed contour

- partially buried by using the FBM/SAA method,” *Progress In Electromagnetics Research*, PIER 76, 253–274, 2007.
5. Wang, M.-J., Z.-S. Wu, and Y.-L. Li, “Investigation on the scattering characteristics of Gaussian beam from two dimensional dielectric rough surfaces based on the Kirchhoff approximation,” *Progress In Electromagnetics Research B*, Vol. 4, 223–235, 2008.
 6. Wang, R. and L. Guo, “Numerical simulations wave scattering from two-layered rough interface,” *Progress In Electromagnetics Research B*, Vol. 10, 163–175, 2008.
 7. Pak, K., L. Tsang, C. H. Chan, and J. T. Johnson, “Backscattering enhancement of vector electromagnetic waves from two-dimensional random rough surfaces based on Monte Carlo simulations,” *J. Opt. Soc. Amer. A, Opt. Image Sci.*, Vol. 12, 2491–2499, 1995.
 8. Du, Y., Y. L. Luo, and J. A. Kong, “Electromagnetic scattering from randomly rough surfaces using the stochastic second-degree method and the sparse matrix/canonical grid algorithm,” *IEEE Trans. Geoscience and Remote Sensing*, Vol. 46, 2831–2839, 2008.
 9. Du, Y., J. C. Shi, Z. Y. Li, and J. A. Kong, “Analysing EM scattering from randomly rough surfaces using stochastic second-degree iterative method, sparse matrix algorithm and Chebyshev approximation,” *Electronics Letters*, Vol. 45, 292–293, 2009.
 10. Li, Q., C. H. Chan, and L. Tsang, “Monte-Carlo simulations of wave scattering from lossy dielectric random rough surfaces using the physics-based two-grid method and canonical grid method,” *IEEE Trans. Antennas Propagat.*, Vol. 47, 752–763, 1999.
 11. Tsang, L., J. A. Kong, K. H. Ding, and C. O. Ao, *Scattering of Electromagnetic Waves, Numerical Simulations*, Vol. 2, Wiley-Interscience, New Jersey, 2001.
 12. Tsang, L., C. H. Chan, K. Pak, and H. Sangani, “Monte-Carlo simulations of large-scale problems of random rough surface scattering and applications to grazing incidence with the BMIA/canonical grid method,” *IEEE Trans. Antennas Propagat.*, Vol. 43, 851–859, 1995.
 13. Chen, K.-S., L. Tsang, and J.-C. Shi, “Microwave emission from two-dimensional inhomogeneous dielectric rough surfaces based on physics-based two-grid method,” *Progress In Electromagnetics Research*, PIER 67, 181–203, 2007.
 14. Holliday, D., L. L. DeRaad, and G. C. St-Cyr, “Forward-backward: A new method for computing low-grazing angle scattering,” *IEEE Trans. Antennas Propagat.*, Vol. 44, 722–729,

- 1996.
15. Iodice, A., "Forward-backward method for scattering from dielectric rough surfaces," *IEEE Trans. Antennas Propagat.*, Vol. 50, 901–911, 2002.
 16. West, J. and J. M. Sturm, "On iterative approaches for electromagnetic rough-surface scattering problems," *IEEE Trans. Antennas Propagat.*, Vol. 47, 1281–1288, 1999.
 17. Liu, B., Z. Y. Li, and Y. Du, "A fast numerical method for electromagnetic scattering from dielectric rough surfaces," submitted for publication.
 18. Chou, H.-T. and J. T. Johnson, "Formulation of forward-backward method using novel spectral acceleration for the modeling of scattering from impedance rough surfaces," *IEEE Trans. Geosci. Remot. Sens.*, Vol. 38, 605–607, 2000.
 19. Chou, H.-T. and J. T. Johnson, "A novel acceleration algorithm for the computation of scattering from rough surfaces with the forward-backward method," *Radio Sci.*, Vol. 33, 1277–1287, 1998.
 20. De Pillis, J., "Faster convergence for iterative solutions to systems via three-part splittings," *SIAM J. Numer. Anal.*, Vol. 15, 888–911, 1978.